Faraday Discussions

Effect of depth of discharge (DOD) on cycling *in situ* formed Li anodes

Journal:	*Faraday Discussions*
Manuscript ID	FD-ART-04-2023-000079.R1
Article Type:	Paper
Date Submitted by the Author:	20-May-2023
Complete List of Authors:	Lee, Kiwoong; University of Michigan, Department of Mechanical Engineering Sakamoto, Jeffrey ; University of Michigan, Department of Mechanical Engineering; University of Michigan, Department of Material Science & Engineering

Title: Effect of depth of discharge (DOD) on cycling *in situ* formed Li anodes

Authors: Kiwoong Lee[1] and Jeff Sakamoto[1,2]*

1Department of Mechanical Engineering, University of Michigan, Ann Arbor, MI 48109, USA

2Department of Material Science & Engineering, University of Michigan, Ann Arbor, MI 48109, USA

*Correspondence: jeffsaka@umich.edu

1. Introduction

Lithium-metal solid-state batteries (LMSSBs) hold great promise as a next-generation battery technology to facilitate the widespread adoption of electric vehicles (EV). Li-metal anodes have a higher theoretical volumetric capacity (2,062 mAh cm^{-3}), compared to conventional graphite-based electrodes (760 mAh cm^{-3}), and exhibit a low electrochemical potential (- 3 V versus standard hydrogen electrode (SHE)) to result in a < 4 V cell voltage when used with a state-of-the-art commercial cathode.[1–6] In addition, by replacing flammable liquid electrolytes (LEs) with solid electrolytes (SEs), the risk associated with a combustible electrolyte is eliminated. Despite these advantages, the development of viable LMSSBs still face several challenges that need to be addressed.

One of the significant challenges with LMSSBs is the issue of Li filament penetration within the SE, which results in short-circuiting. Even when using ceramic electrolytes, which have adequate stiffness to physically stabilize the Li surface, Li filament growth is known to occur above a critical current density (CCD).[7–9] Consequently, numerous studies have focused efforts to understand the mechanisms of Li penetration to increase the CCD. [10–16]

However, an emergent phenomena arises when the Li-metal anode is stripped during discharge. Unlike Li/LE interfaces where the LE conforms to the Li surface, Li/SE interfaces require Li replenishment by diffusion or viscoplastic deformation under pressure to maintain homogeneous contact at the interface. When the Li replenishment rate is insufficient, depletion of Li at the interface, such as de-wetting or void formation, occurs.[17–19] Inhomogeneous current density in the void proximity leads to a “current constriction effect”, as proposed by Eckhardt *et al* .[20], resulting in an increase in interfacial resistance between Li and the SE.[20–22] As the interface resistance increases, cell polarization results in a dramatic

drop in cell potential, thus reducing the accessible or discharge capacity.[22] Additionally, interfaces with voids cause local current focusing near the edges of voids during subsequent charging cycles, leading to Li filament penetration at lower current densities than the CCD.[17]

Higher stack pressure[19] and elevated temperature[23] have been suggested to address this issue by enhancing the creep flow of Li. For example, Jolly *et al.* demonstrated that increasing the temperature from 25°C to 80°C can increase the stripping CCD for void formation from <0.25 mA cm^{-2} to >0.5 mA cm^{-2}, respectively.[23] Moreover, interlayers or alloying anodes[24] have been suggested to maintain a homogeneous Li/SE interface during cycling. For example using Ag-C composite interlayer between Li and SE has been reported to maintain homogeneous Li flux at the interface in extended cycling tests.[25,26] Similarly, Fuchs *et al.* have enabled stable Li stripping for over 20 mAh cm^{-2} without external stack pressure by using Li-carbon nanotubes composite electrodes.[27] It was believed that the carbon nanotubes enhance Li diffusivity at the interface, to maintain homogeneous Li flux during stripping.

Despite significant efforts to understand the mechano-electrochemical behavior of Li anodes at Li/SE interfaces, the majority of studies have been limited to using thick Li foil. However, to achieve energy densities exceeding those of state-of-the-art Li-ion batteries, thin Li-metal anodes with the thickness between 15 - 30 µm is necessary.[28] Recently, “Anode-free” manufacturing, in which the cell is assembled in a discharged state with no metallic Li, is garnering interest. This approach for forming thin Li-metal anodes[26,29] is appealing owing to its potential to reduce manufacturing costs. In addition, *in situ* formation of Li-metal anodes through anode-free manufacturing provides enhanced purity due to the ion selectivity of SEs. The increase in purity can improve viscoplastic behavior and diffusivity, both of which are beneficial for Li cycling performance.

However, as reported by several studies[30–32], the mechanical behavior of Li-metal anodes depends on their thickness. In a recent study of the Li/$Li_7La_3Zr_2O_{12}$ (LLZO) interface, as the thickness of Li decreased, the effect of hydrostatic pinning increased due to the adhesion between Li metal layer and LLZO, thus impeding Li flow.[30] As a result, *in situ* formed Li anodes with a thickness in the range of 10 – 30 µm exhibit significant different mechano-electrochemical behaviors than lab-scale thick Li foil (> 50 µm). Moreover, as *in situ* formed Li is cycled, the relative changes in Li thickness are more significant compared to Li foil,[32] indicating that the mechanical behavior of *in situ* formed Li anodes change significantly during cycling.

In previous work, we demonstrated that there are significant differences in the stripping behavior of *in situ* plated Li electrodes compared to thick Li foil.[22] Specifically, as the thickness of *in situ* formed Li decreased during stripping, the rate of Li replenishment also decreased. This continuous decrease in the replenishment rate during stripping led to a transition from quasi-stable stripping, where Li flux was balanced at the interface, to unstable stripping, where Li flux imbalance occurred. At the onset of unstable stripping, significant void formation occurs. Moreover, the accessible capacity, where this transition between quasi and unstable stripping occurred, increased as the stripping current densities increased and the Li thickness decreased. While this study shed light on understanding the stripping behavior of thin *in situ* Li anodes in unidirectional tests, the cycling behavior (repeated stripping and plating) has not yet been characterized.

It has been reported that voids are not fully refilled during cycling of Li.[17] In the case of cycling *in situ* formed Li anodes, the pore area/volume will increase at the interfaces during stripping as the depth of discharge (DOD) increases. We believe that when these pores are relatively small, the current focusing around the voids is not significant and thus do not lead to the acceleration of void growth. However, with repeated cycling and as a result of the lack of back-filling or re-wetting of the SE interface, the voids can accumulate with each cycle and grow into large voids causing unstable stripping resulting in significant polarization. Consequently, the cycling of *in situ* formed Li-metal anodes is exacerbated as the DOD increases, thus limiting the accessible discharge capacity. Altogether, to better understand the commercial potential of Li anodes made using the anode-free approach, there is a need to study the effect of DOD on the cycling behavior of *in situ* formed Li electrodes.

This study aims to understand the cycling behavior of *in situ* Li as a function of DOD. LLZO was used as a model electrolyte owing to its high ionic conductivity (~ 1 mS cm^{-1}) and excellent stability against Li metal. To study the effect of DOD on cycling, the *in situ* Li anode thickness was fixed at 3 mAh/cm^2 or 15 µm, and the DOD was varied between 33 and 66% by changing the cycling capacity. The accumulation of interfacial degradation (void formation and loss of contact) as a function of DOD was observed by *ex situ* cross-sectional analysis of Li/LLZO interfaces and laser profilometry. Additionally, to further investigate the effect of DOD on cycling *in situ* Li anodes, a fixed capacity of Li (2 mAh cm^{-2}) was cycled with different initial total capacities in the range of 3 to 8 mAh cm^{-2}. Finally, to see the effect of the current densities on cycling *in situ* Li, cycling *in situ* Li with fixed DOD was conducted over a range of current densities. The results of this study not only improve the understanding of cycling behavior of LMSSBs

with the anode-free configuration ,but also suggest guidelines to improve the cycling of *in situ* formed Li anodes.

2. Results and Discussion

To investigate the cycling behavior of *in situ* formed Li anodes, a custom cell design was used (Figure 1). A battery-grade copper (Cu) current collector (CC) with thickness of 10 µm was laminated on LLZO pellet by following the method reported by Wang *et al*.[29] An *in situ* Li layer was then formed between the Cu CC and LLZO pellet by electrochemically transferring Li from the thick Li foil counter electrode by applying pulsed current at 60°C and 4.2 MPa (See methods for details).

Kazyak *et al.* has shown that inhomogeneity in the Li plating can occur due to nonuniform nucleation and growth of *in situ* plated Li.[33] To mitigate the issue of nonuniformity of *in situ* Li, which can limit the amount of the Li that can be stripped, and impact the cycling properties, we used high-rate pulsed current to enable uniform nucleation of Li as the adhesion force between Cu CC and LLZO became less significant.[34] In addition, *in situ* plating was performed at a higher temperature (60°C, homologous temperature: 0.73) to reduce the flow stress of Li during *in situ* plating, thereby enhancing the uniformity of *in situ* Li. Cross-sectional scanning electron microscope (SEM) images of Li/LLZO interfaces cut by forced ion beam (FIB) after *in situ* plating (Figure S1) confirm that Li was uniformly plated regardless of the area in which Li was plated *in situ*.

After formation of *in situ* Li, a certain amount of Li was galvanostatically cycled as a function of DOD to characterize the effect of DOD on cycling behavior of *in situ* Li. Tests were terminated if voltage responses abruptly increased due to interfacial depletion of Li, such as void formation or de-wetting, and reached the cutoff voltage (2.0 V) limiting discharge capacity. All the cycling tests were conducted at 60°C (±3°C) under a stack pressure of 4.2 MPa. The use of elevated temperature allowed the use of current densities that reduced the propensity for Li filament penetration and catastrophic cell short-circuiting, thus resulting in more time-efficient cycling test.

2.1. Effect of DOD at fixed in situ Li plated capacity

To study the effect of DOD on the cycling behavior of *in situ* formed Li anodes, *in situ* formed Li anodes were cycled with different capacities using a current density of 0.75 mA cm^{-2} after *in situ* plating of 3 mAh cm^{-2}(~ 15 µm).

Previous research has shown that void formation at the Li/LLZO interfaces during stripping can cause irreversible deterioration due to de-wetting. We believe the re-wetting of the LLZO with Li cannot be fully established solely by stack pressure and subsequent plating unless additional treatments, such as heat treatment is used.[22] Therefore, to prevent void formation during the first stripping half-cycle and termination of the test due to an abrupt increase in voltage and reaching the voltage cutoff, cycling capacity should be lower than the accessible capacity where the void formation and its growth at the interface are accelerated. Accordingly, we performed unidirectional stripping of *in situ* Li of 3 mAh cm^{-2} (~ 15 µm-thick) at 0.75 mA cm^{-2} to evaluate the accessible capacity. To determine the accessible capacity, we conducted unidirectional stripping of *in situ* Li of 3 mAh cm^{-2} at 0.75 mA/cm^2, and determined the capacity using the second derivatives of the stripping voltage profile, following the method reported in a previous study. (Figure S2) The accessible capacity was found to be ~2.5 mAh cm^{-2}. Therefore, we set the cycling capacity as 1, 1.5, and 2 mAh cm^{-2}, all of which were below the accessible capacity (2.5 mAh cm^{-2}).

Figure 2 shows the voltage responses for *in situ* Li with different cycling capacities, which were 1, 1.5 and 2 mAh cm^{-2}, corresponding to DOD of 33%, 50% and 66 %, respectively. Positive and negative voltage responses indicate Li stripping and plating on the *in situ* electrode, respectively. Taylor *et al.* previously demonstrated that thick Li foil electrodes exhibited stable and ohmic voltage behavior when cycling at 1 mA cm^{-2}, 3.3 MPa and 60°C[15], which were less aggressive cycling conditions than those used in this study. Thus, any significant changes in voltage were attributed to interfacial changes of the *in situ* Li electrode. As shown in Figure 2A, at a DOD of 33%, the voltage responses remained stable for 60 cycles. Although a slight increase in voltage was observed during stripping *in situ* Li (Figure S3), the voltage was recovered during the subsequent plating half-cycle resulting in stable cycling. This can be an indication that small-sized pores formed at the interface during stripping, but the size of the pores was not significantly large, such that they were annihilated during the subsequent plating as computationally demonstrated by Zhao *et al*.[35]

However, as shown in Figure 2B and C, at DODs of 50% or 66%, dramatic polarization was observed during cycling. Furthermore, as the DOD increased, the voltage polarization appeared earlier. When the DOD was 66% (Figure 3C), a noticeable increase in voltage appeared at the second stripping half-cycle, and voltage reached the voltage cut-off at the third stripping cycle, limiting the discharge capacity to 1.8 mAh cm^{-2}.

At a DOD of 50% (Figure 3B), intermediate cycling behavior between 33% and 66% was observed. Voltage responses were relatively stable until the 21st cycle, followed by noticeable polarization appearing at the 22nd cycle. Compared to the DOD of 66% cycling, the degree of polarization was relatively subtle and did not limit the discharge capacity. The degree of polarization then increased every cycle for 15 cycles and reached the voltage cutoff (2 V) limiting the discharge capacity.

It is worth noting that even though the cycling capacities of 1.5 or 2.0 mAh cm^{-2} were below the accessible capacity of 3 mAh cm^{-2} *in situ* Li (~2.5 mAh cm^{-2}), which was evaluated from unidirectional stripping, there was an abrupt increase in voltage response during stripping after repeating several cycles. This indicates contact loss at the interface likely accumulated with every cycle leading to severe Li depletion and void formation, as previously suggested by previous studies.[17,23] In the case of *in situ* thin Li electrodes, as the DOD increases, the Li inhomogeneity increases, leading to unstable flux (current focusing) in the proximity of Li voids.

To investigate the interfacial morphologies of *in situ* Li with cycling as a function of DOD, we performed *ex situ* cross-sectional FIB-SEM analysis (Figures 3 and 4). Figure 3 shows the cross-sectional images after cycling *in situ* Li with a DOD of 33%, which exhibited stable cycling behavior as shown in Figure 2A. Figure 3A-C represents the Li/LLZO interface after completing the 30th stripping half-cycle at different areas of the *in situ* Li electrode. As shown in Figure 3A-C, the thickness of *in situ* Li was uniformly ~ 10 µm (2 mAh cm^{-2}) irrespective of the investigated area, indicating that 1 mAh cm^{-2} of Li was uniformly stripped from 3 mAh cm^{-2} after 30 cycles. Additionally, there was no evidence of noticeable void formation at Li/LLZO interfaces, which is consistent the lack of significant abrupt increase in voltage during cycling.

The same cells (33% DOD) was analyzed after the 30th plating half-cycle (Figure 3D-F). Regardless of the investigated area, Li had a uniform thickness of ~15 µm (~3 mAh cm^{-2}). As *in situ* Li was stripped uniformly and conformed to the LLZO surface after stripping (Figure 3A-C), Li was plated homogeneously. Small-sized pores, which were too small to be observed by SEM, likely formed at Li/LLZO interfaces during the stripping half-cycle, as a slight increase in voltage during stripping was observed (Figure S3). We believe this behavior is consistent with what previously was referred to as quasi-stable stripping.[22] However, considering that Li was plated homogeneously, it was expected that these pores essentially were annihilated or back-filled with Li, thus resulting in stable cycling.

We also investigated the Li/LLZO interfaces of the cell after cycling with a DOD of 66% (Figure 4). The same cell shown in Figure 2C, where a dramatic voltage polarization appeared at the third stripping half-cycle, was used to analyze the interfaces after cycling (Figure 4A-C). Contrary to the cross-section of the cell cycled at DOD of 33% (Figure 3), severe inhomogeneity of Li layer was observed. Some areas of the Li/LLZO interfaces (Figure 4A) showed conformal and uniform coating of Li on LLZO with no noticeable evidences of interfacial degradation, such as void formation. However, severe Li depletion was observed in other areas as shown in Figure 4B and C. The thickness of Li shown in Figure 4A was around 6.8 μm, thicker than the expected thickness, which was ~ 6 μm (1.2 mAh cm^{-2}) if the stripping was performed uniformly.

To further investigate the interfacial deterioration resulting from cycling at DOD of 66%, the cell was examined after plating on deteriorated interface as shown in Figure 4A-C. Corresponding voltage profiles can be found in Figure S4. Three distinct types of Li/LLZO interfaces were observed from its cross-sectional SEM images. Firstly, some areas showed conformal and uniform Li plating on LLZO (Figure 4D), likely from plating Li on the conformal interfaces as shown in Figure 4A. Secondly, in some areas complete disconnection occurred between the Cu CC and LLZO. Finally, the large-scale voids were observed as shown in Figure 4E with a lateral size greater than 20 μm. Compared to our previous study[22] in which *in situ* Li was only unidirectionally stripped, the interfacial degradation when cycling was significantly worse due to the accumulation of void formation. The size of voids was also remarkably larger. Considering that the size of voids are in the range of a few μm when Li was stripped once[13,22], the size of void after repeated cycling was greater than 10 μm.

Also, to verify if this phenomena was attributed to the accumulation of void formation from cycling, Li/LLZO interfaces were investigated after the first stripping half-cycle. Figure S5 shows the cross-sectional images of Li/LLZO interfaces after the first stripping half-cycle, showing that no noticeable evidence of void formation was observed. Therefore, we can conclude that by repeating stripping and plating with a high DOD, the inhomogeneity at the interface accumulated over numerous cycles, leading to severe interfacial deterioration (Figure 4B and C).

Additionally, we note that Li penetration into LLZO was observed (red circle in Figure 4F). Li filaments were located near the edge of the void. This indicated that Li filament penetration as a result of current focusing at the edge of the voids as suggested by Kasemchainan *et al*.[17] Also, despite the conformal coating of Li on LLZO without any evidence of void formation (Figure 4D), Li filament penetration was

observed. This could be attributed to the effect of cycling capacity as reported by Lewis *et al.*[36] where as the amount of Li cycled increases, Li filament penetration is more likely to occur. Moreover, as the effective area decreased due to the growth of voided/de-wetted area, increased local current resulted in Li filament penetration. Although the depth of penetration was in the range of only few micrometers which was hardly detectable from its voltage responses, it could impact long-term cycling as it can grow further with each cycle leading to cell short-circuiting.

To investigate the *in situ* Li anode homogeneity in the 66% DOD, morphological changes of the Cu CC free surface were analyzed. It was assumed that any significant changes in the Cu CC morphology after cycling were a result of changes in the *in situ* Li morphology or homogeneity. To achieve this, the Cu CC free surfaces were scanned with a laser confocal microscope. Each confocal microscope measurement covered an area of 650 x 650 μm^2, which was approximately 1.3 % of the total electrode area (0.317 cm^2). To examine the effect of cycling at the highest DOD (66%) in this study, the cell was first scanned after *in situ* plating (Figure 5A) and then scanned again after cycling at a DOD of 66% (Figure 5B). Several positions on the electrode surface were scanned in each condition. As shown in Figure 5A, Li layer was *in situ* plated uniformly without any significant nonuniformity. However, after cycling at a DOD of 66%, significant nonuniformity was observed with several pits, as shown in Figure 5B. We assumed these pits in the Cu CC were directly above Li voids. Furthermore, a large pit with a lateral size of ~ 300 µm in Figure 5B (iii) was ~3 - 4 µm lower than surrounding area, indicating the formation of a large void.

As shown above in Figure 3-5, cycling *in situ* Li with a DOD of 66% resulted in severe deterioration at the Li/LLZO interfaces and significant nonuniformity of *in situ* Li layer, whereas cycling with a DOD of 33% did not exhibit any noticeable evidence of void formation and nonuniformity. As previously demonstrated, as *in situ* Li is stripped, more pores form and grow at the interfaces since the Li replenishment rate decreases.[22] As a result, compared to cycling with a DOD of 33%, cycling with a DOD of 66% resulted in more pores at the interfaces and their size was sufficiently large such that they could not be backfilled by subsequent plating of Li or by stack pressure.[35] At the subsequent stripping half-cycle, currents were focused near the edge of remaining voids, promoting the further growth of voids. By repeating these processes, we believe small voids eventually grew into large voids. As the size of voids increased, the degree of current focusing became more significant, leading to Li filament

penetration, as shown in Figure 4F. In addition, since voids formed during the stripping and Li was not plated at the voided area during the subsequent plating, there appeared to be a height difference between the voided area and non-voided area as shown in Figure 5B and C. The voids in the Li layer would result in nonuniform stress at the interfaces, affecting the kinetics of the interfacial reactions, such as Gibbs free energy, equilibrium potential and exchange current density.[37,38] Also, the combination of tensile internal stress of Cu CC induced by the height difference of Li layer and the adhesion between Cu CC and Li layer was likely to hinder Li flow to the interfaces during stripping, resulting in more void formation. Therefore, a deeper investigation including mechanical factors such as adhesion between the Li and Cu CC, changes in mechanical properties of the Li during cycling and internal stress of Cu CC due to the nonuniformity can provide more mechanistic insight into what controls Li void formation during the cycling of thin *in situ* Li.

2.2 Effect of DOD at fixed cycling capacity

To more accurately determine whether reducing the DOD can improve the cycling stability, *in situ* Li was cycled with a constant cycling capacity, while varying the *in situ* plated capacity. As discussed earlier and shown in Figure 2, when cycling 2 mAh cm^{-2} after *in situ* plating 3 mAh cm^{-2} resulted in a dramatic increase in voltage during the third stripping half-cycle, which limited the discharge capacity. Thus, we varied the *in situ* plated capacity between 3 and 8 mAh cm^{-2} to investigate whether cycling *in situ* Li of 2 mAh cm^{-2} can be stabilized by lowering the DOD. Figure 6 shows the voltage profiles of cycling 2 mAh cm^{-2} of *in situ* Li with initially plated amounts of Li of 3, 4, and 8 mAh cm^{-2}, corresponding to DODs of 66% (green), 50% (red) and 25% (blue), respectively. The results showed that as DOD decreased, the stability of cycling was enhanced.

When 2 mAh cm^{-2} was cycled at a DOD of 50% (*in situ* plated Li of 4 mAh cm^{-2}), the cycling was relatively stable for the first 5 cycles after which the noticeable increase in voltage was observed. The degree of voltage polarization was then increased with each cycle, similar to the behavior observed when cycling 1.5 mAh cm^{-2} of total capacity of 3.0 mAh cm^{-2} (Figure 2B). Moreover, when the total capacity was increased to 8 mAh cm^{-2}, the voltage was relatively stable for 20 cycles, indicating improved suppression of void formation. A slight increase in voltage was observed at the 15th to 20th cycles, and the degree of polarization increased slowly with each cycle, but compared to other two cases, cycling remained more stable. The results demonstrate that reducing DOD by increasing the total capacity of *in situ* plated Li at a fixed cycling capacity resulted in more stable cycling. This finding aligns with the results shown in

Figure 2 that reducing DOD by decreasing the cycling capacity at a fixed total capacity also led to more stable cycling.

It has been shown that as the thickness of Li increases, void formation is suppressed.[22] Therefore, as the total capacity of *in situ* Li anodes increased, the Li/LLZO interface maintained homogeneous contact after stripping 2 mAh cm^{-2}. Moreover, although voids likely formed after each stripping half-cycle, thicker remaining Li was more advantageous in suppressing severe void formation. We believe the flow of Li through creep is more likely to occur as the Li thickness increases. Therefore, as the capacity of *in situ* plating increased, while keeping the amount of Li cycled fixed, it was shown the cycling stability improved.

Additionally, 750 µm-thick Li foil was cycled with a cycling capacity of 2 mAh cm^{-2} using a thick Li/LLZO/thick Li symmetric cell (Figure S6A) to examine the case where the cycling capacity was significantly smaller compared to the total capacity (~ 1%). As shown in Figure S6A, cycling of thick Li foil was stable for 40 cycles without any noticeable voltage increase. Moreover, while cycling *in situ* Li exhibited a slight increase in voltage responses even when cycling was stable (Figure 2A and Figure S3), thick Li showed an almost flat or ohmic voltage response for the entire 40 cycles as shown in Figure S6B, indicating a lower propensity for void formation during cycling. While the cycling performance of 2 mAh cm^{-2} ostensibly appears impressive, only 1% of the Li capacity is used, which is not commercially-relevant. From a mechanistic perspective, cycling of thick Li foil cannot be directly compared to that of *in situ* formed Li layer since it exhibits different mechano-electrochemical properties due to its different properties, such as microstructure, purity and interfacial chemistry. Nonetheless, the result suggests that increasing the thickness of Li can improve the stability of cycling which is consistent with the results shown in Figure 6.

2.3. Effect of current density

Finally, to investigate the impact of current density on cycling *in situ* Li anodes, cells cycled 2 mAh cm^{-2} of 3 mAh cm^{-2} *in situ* Li with different current densities in the range of 0.4 – 0.75 mA cm^{-2}. Figure 7 shows the voltage profiles of cycling with each current densities. As previously mentioned in Figure 2 and 6, when Li was cycled at 0.75 mA cm^{-2}, instability of cycling appeared earlier in the cycling tests, specifically at the third cycle. When the current density was 0.5 mA cm^{-2}, the stability of cycling was relatively improved, and the degree of voltage polarization increased more gradually in comparison to

cycling at 0.75 mA cm^{-2}. When the current density was lowered to 0.4 mA cm^{-2}, stable cycling was achieved for 10 cycles.

As the current density decreases during stripping, it is likely that the suppression of void formation improved. As a result, lower current densities enabled the stable cycling without void formation and their accumulated effect on cycling stability. This indicates that as current density increases, the tolerable DOD decreases. Furthermore, when *in situ* Li is stripped at sufficiently low current densities, Li flux balance at the interface is maintained to the extent that the full capacity of the Li anode is utilized.[22] This suggests that when the cycling current density is lower than a threshold current density, at which stripping is limited by Li depletion, stable cycling with higher DOD can be achieved. Thus, in future studies it will be important to determine and understand the origin of this threshold current density for void formation.

3. Methods

3.1. Cell Preparation

Ta-doped cubic phase LLZO with nominal composition $Li_{6.5}La_3Zr_{1.5}Ta_{0.5}O_{12}$ was synthesized by a solid-state synthetic method from starting powders of Li_2CO_3 (Alfa Aesar), La_2O_3 (PIDC), ZrO_2 (Inframat Advanced Materials), and Ta_2O_5 (Inframat Advanced Materials). LLZO powders were consolidated into a LLZO pellet with a diameter of 12.7 mm by using rapid induction hot pressing (RIHP) under 47.32 MPa at 1225°C for 40 minutes. The resulting LLZO pellets were cut into ~2 mm thick pellets using a diamond saw. X-ray diffraction (XRD) measurements of resulting pellets were performed to verify the phase purity of hot-pressed LLZO. As shown in Figure S7, the phase purity was high without any evidence of the tetragonal phase. One side of the pellets was dry-polished using 400, 600 and 1200 grit sandpapers. A 10 µm thick Cu foil (Targray) with a diameter of 6.35 mm was then laminated on the polished side of the LLZO pellet by applying 3.15 MPa at 900 °C for 5 minutes under an Argon atmosphere. After lamination, the other side of the LLZO pellet was polished with a series of decreasing grit sandpaper and diamond pastes with a final polish of 0.1 µm. The Cu/LLZO cell was then heat-treated at 400 °C for 4 hours in an Argon atmosphere glove box to remove any Li_2CO_3 contamination. Li foil (750 µm thick, Alfa Aesar) of a diameter of 6.35 mm was attached on the 0.1 µm polished side and heated to ~170 °C for 12 hours to obtain low interfacial resistance between thick Li foil and LLZO (<10 Ω cm^2).

3.2. Electrochemical methods

All electrochemical methods were performed using a Bio-logic VMP-300 galvanostat/potentiostat under inert atmospheric conditions at 60°C. Cells were compressed under a constant uniaxial pressure of 4.2 MPa during the entire electrochemical tests by using a mechanical force gauge (Imada) and home-made fixture. *In situ* Li of 3-8 mAh cm^{-2} (~15 - 39 µm thick) was electrochemically plated from thick Li foil source electrode to Cu CC*. In situ* Li anodes were made using the procedures in reference 34.[34]

3.3. Characterization

Cross-sectional SEM images were obtained using a Helios G4 PFIB UXE dual beam system (Thermo Fisher). FIB milling was performed using Ga^+ ions with an acceleration voltage of 30 kV and ion beam current of 0.5 µA. SEM images were than obtained with an acceleration voltage of 2 kV and beam current of 0.1 nA.

3D images of the surface morphology of *in situ* Li layer covered by Cu foil were acquired by a laser confocal microscope (Olympus OLS 4000 LEXT) with 20x confocal objectives (MPLAPON20XLEXT).

4. Conclusion

This work investigated the effect of DOD on the cycling performance of *in situ* formed Li anodes. First, the effect of DOD on cycling behavior was studied. The results indicated that as DOD increased cycling stability decreased. We believe that as the DOD increased, the instability of voltage appeared during the stripping half-cycle at earlier cycles leading to reduced discharge capacity. For example, stable cycling was observed for 60 cycles when 1 mAh cm^{-2} of Li was cycled after *in situ* plating of 3 mAh cm^{-2} (DOD of 33%). However, the cycling stability ended at the 3rd stripping half-cycle when using a cycling capacity of 2 mAh cm^{-2} (DOD of 66%). The *ex situ* investigation of Li/LLZO interfaces revealed the accumulation of Li inhomogeneity at the LLZO interface. The effect of DOD was further investigated by cycling a constant capacity with different total initial capacities. It was also shown that reducing the DOD by increasing the total capacity from 3 mAh cm^{-2} (DOD of 66 %) to 8 mAh cm^{-2} (DOD of 25 %) improved the cycling stability. Finally, the effect of current density was investigated. It was shown that as current density increased, the DOD decreased. For example, while cycling 2 mAh cm^{-2} with a DOD of 66 % at 0.75 mAh cm^{-2} unstable cycling was observed. However, when cycling 2 mAh cm^{-2} with a DOD of 66 % at a lower current density of 0.4 mA cm^{-2}, stable cycling was achieved over 10 cycles.

This study shows that when cycling *in situ* Li anodes of anode-free cells, cycling at lower DODs improves cycling behavior. However, DOD is inversely proportional with the energy density. For example at 60°C, a stack pressure of 4.2 MPa, and a current density of 0.75 mA cm^{-2}, a total capacity of over 8 mAh cm^{-2} is required for the stable cycling of 2 mAh cm^{-2}. Therefore, to enhance the energy density of anode-free LMSSBs by improving the DOD for the stable cycling, it is necessary to develop approaches to improve stripping capacity while suppressing void formation. One potential method to enhance the DOD for the cycling stability is to utilize higher stack pressure and temperature, as they have been shown to enhance stripping capacity.[19,23,39,40] Moreover, to mitigate the issue of void formation with increasing DOD, additional interfacial treatments, such as heat treatment to heal the Li/LLZO interface[22] can be suggested. These findings provide insights into the development of high-performance LMSSBs manufactured using the anode-free configuration.

Author Contributions

K.L.: conceptualization, validation, formal analysis, investigation, resources, data curation, writing-original draft, writing – review & editing and visualization. J.S.: conceptualization, writing – review & editing, supervision and funding acquisition.

Conflicts of interest

J.S. is the founder of Zakuro, Inc. J.S. is a contributor on a patent related to the methods used to *in situ* form the Li-metal anodes in this study, “Method of Method of Electrodeposition of Electroactive Species at Solid-Solid Interfaces,” 2021/150683 A1, 20210226193.

Acknowledgements

K.L and J.S acknowledge support from the U.S. Department of Energy (DOE)’s Office of Efficiency and Renewable Energy (EERE) and Vehicle Technologies Office (VTO) under contract DE-EE 00008855. The authors acknowledge the financial support of the University of Michigan College of Engineering and technical support from the Michigan Center for Materials Characterization. K.L. acknowledges support from the Kwanjeong Educational Foundation.

References

1 J. Janek and W. G. Zeier, *Nat Energy*, 2016, **1**, 1–4.
2 Y. Kato, S. Hori, T. Saito, K. Suzuki, M. Hirayama, A. Mitsui, M. Yonemura, H. Iba and R. Kanno, *Nat Energy*, 2016, **1**, 1–7.
3 A. L. Robinson and J. Janek, *MRS Bulletin*, 2014, **39**, 1046–1047.
4 J.-M. Tarascon and M. Armand, *Nature*, 2001, **414**, 359–367.
5 P. Albertus, S. Babinec, S. Litzelman and A. Newman, *Nat Energy*, 2018, **3**, 16–21.
6 J. B. Goodenough and Y. Kim, *Chem. Mater.*, 2010, **22**, 587–603.
7 A. Sharafi, H. M. Meyer, J. Nanda, J. Wolfenstine and J. Sakamoto, *Journal of Power Sources*, 2016, **302**, 135–139.
8 R. Raj and J. Wolfenstine, *Journal of Power Sources*, 2017, **343**, 119–126.
9 L. C. Zhang, J. F. Yang, C. L. Li, Y. X. Gao, X. P. Wang and Q. F. Fang, *Journal of Power Sources*, 2020, **449**, 227610.
10 L. Porz, T. Swamy, B. W. Sheldon, D. Rettenwander, T. Frömling, H. L. Thaman, S. Berendts, R. Uecker, W. C. Carter and Y.-M. Chiang, *Advanced Energy Materials*, 2017, **7**, 1701003.
11 T. Swamy, R. Park, B. W. Sheldon, D. Rettenwander, L. Porz, S. Berendts, R. Uecker, W. C. Carter and Y.-M. Chiang, *Journal of The Electrochemical Society*, 2018, **165**, A3648.
12 X. Liu, R. Garcia-Mendez, A. R. Lupini, Y. Cheng, Z. D. Hood, F. Han, A. Sharafi, J. C. Idrobo, N. J. Dudney, C. Wang, C. Ma, J. Sakamoto and M. Chi, *Nat. Mater.*, 2021, **20**, 1485–1490.
13 E. Kazyak, R. Garcia-Mendez, W. S. LePage, A. Sharafi, A. L. Davis, A. J. Sanchez, K.-H. Chen, C. Haslam, J. Sakamoto and N. P. Dasgupta, *Matter*, 2020, **2**, 1025–1048.
14 G. T. Hitz, D. W. McOwen, L. Zhang, Z. Ma, Z. Fu, Y. Wen, Y. Gong, J. Dai, T. R. Hamann, L. Hu and E. D. Wachsman, *Materials Today*, 2019, **22**, 50–57.
15 N. J. Taylor, S. Stangeland-Molo, C. G. Haslam, A. Sharafi, T. Thompson, M. Wang, R. Garcia-Mendez and J. Sakamoto, *Journal of Power Sources*, 2018, **396**, 314–318.
16 K. (Kelvin) Fu, Y. Gong, G. T. Hitz, D. W. McOwen, Y. Li, S. Xu, Y. Wen, L. Zhang, C. Wang, G. Pastel, J. Dai, B. Liu, H. Xie, Y. Yao, E. D. Wachsman and L. Hu, *Energy Environ. Sci.*, 2017, **10**, 1568–1575.
17 J. Kasemchainan, S. Zekoll, D. S. Jolly, Z. Ning, G. O. Hartley, J. Marrow and P. G. Bruce, *Nature materials*, 2019, **18**, 1105–1111.
18 T. Krauskopf, H. Hartmann, W. G. Zeier and J. Janek, *ACS Appl. Mater. Interfaces*, 2019, **11**, 14463–14477.
19 M. J. Wang, R. Choudhury and J. Sakamoto, *Joule*, 2019, **3**, 2165–2178.
20 J. K. Eckhardt, P. J. Klar, J. Janek and C. Heiliger, *ACS Appl. Mater. Interfaces*, 2022, **14**, 35545–35554.
21 H. Koshikawa, S. Matsuda, K. Kamiya, M. Miyayama, Y. Kubo, K. Uosaki, K. Hashimoto and S. Nakanishi, *Journal of Power Sources*, 2018, **376**, 147–151.
22 K. Lee, E. Kazyak, M. J. Wang, N. P. Dasgupta and J. Sakamoto, *Joule*, 2022, **6**, 2547–2565.
23 D. Spencer Jolly, Z. Ning, G. O. Hartley, B. Liu, D. L. R. Melvin, P. Adamson, J. Marrow and P. G. Bruce, *ACS Appl. Mater. Interfaces*, 2021, **13**, 22708–22716.
24 J. A. Lewis, K. A. Cavallaro, Y. Liu and M. T. McDowell, *Joule*, 2022, **6**, 1418–1430.
25 J.-S. Kim, G. Yoon, S. Kim, S. Sugata, N. Yashiro, S. Suzuki, M.-J. Lee, R. Kim, M. Badding, Z. Song, J. Chang and D. Im, *Nat Commun*, 2023, **14**, 782.
26 Y.-G. Lee, S. Fujiki, C. Jung, N. Suzuki, N. Yashiro, R. Omoda, D.-S. Ko, T. Shiratsuchi, T. Sugimoto, S. Ryu, J. H. Ku, T. Watanabe, Y. Park, Y. Aihara, D. Im and I. T. Han, *Nat Energy*, 2020, **5**, 299–308.
27 T. Fuchs, C. G. Haslam, A. C. Moy, C. Lerch, T. Krauskopf, J. Sakamoto, F. H. Richter and J. Janek, *Advanced Energy Materials*, 2022, **12**, 2201125.
28 M. J. Wang, E. Kazyak, N. P. Dasgupta and J. Sakamoto, *Joule*, 2021, **5**, 1371–1390.

29 M. J. Wang, E. Carmona, A. Gupta, P. Albertus and J. Sakamoto, *Nat Commun*, 2020, **11**, 5201.
30 C. G. Haslam, J. B. Wolfenstine and J. Sakamoto, *Journal of Power Sources*, 2022, **520**, 230831.
31 A. Masias, N. Felten and J. Sakamoto, *Journal of Materials Research*, 2021, **36**, 729–739.
32 W. S. LePage, Y. Chen, E. Kazyak, K.-H. Chen, A. J. Sanchez, A. Poli, E. M. Arruda, M. D. Thouless and N. P. Dasgupta, *J. Electrochem. Soc.*, 2019, **166**, A89.
33 E. Kazyak, M. J. Wang, K. Lee, S. Yadavalli, A. J. Sanchez, M. D. Thouless, J. Sakamoto and N. P. Dasgupta, *Matter*, 2022, **5**, 3912–3934.
34 United States, US20210226193A1, 2021.
35 Y. Zhao, R. Wang and E. Martínez-Pañeda, *Journal of the Mechanics and Physics of Solids*, 2022, **167**, 104999.
36 J. A. Lewis, C. Lee, Y. Liu, S. Y. Han, D. Prakash, E. J. Klein, H.-W. Lee and M. T. McDowell, *ACS Appl. Mater. Interfaces*, 2022, **14**, 4051–4060.
37 M. Ganser, F. E. Hildebrand, M. Klinsmann, M. Hanauer, M. Kamlah and R. M. McMeeking, *J. Electrochem. Soc.*, 2019, **166**, H167.
38 E. A. Carmona, M. J. Wang, Y. Song, J. Sakamoto and P. Albertus, *Advanced Energy Materials*, 2021, **11**, 2101355.
39 J. A. Lewis, S. E. Sandoval, Y. Liu, D. L. Nelson, S. G. Yoon, R. Wang, Y. Zhao, M. Tian, P. Shevchenko, E. Martínez-Pañeda and M. T. McDowell, *Advanced Energy Materials*, 2023, **13**, 2204186.
40 M. Wang, J. B. Wolfenstine and J. Sakamoto, *Electrochimica Acta*, 2019, **296**, 842–847.

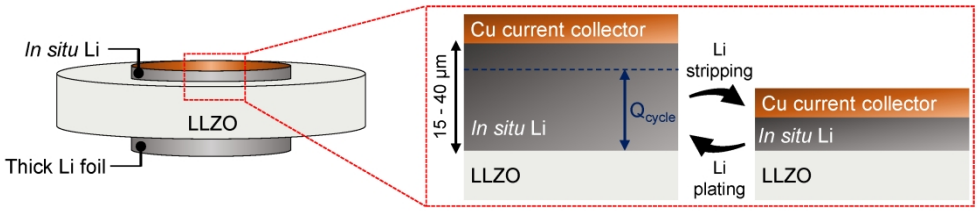

Figure 1. A schematic illustration of anode-free cell configurations.The custom-made *in situ* Li/ LLZO/thick Li foil cell (left) and a zoomed-in view of how the *in situ* Li/LLZO interface operates during cycling.

140x30mm (600 x 600 DPI)

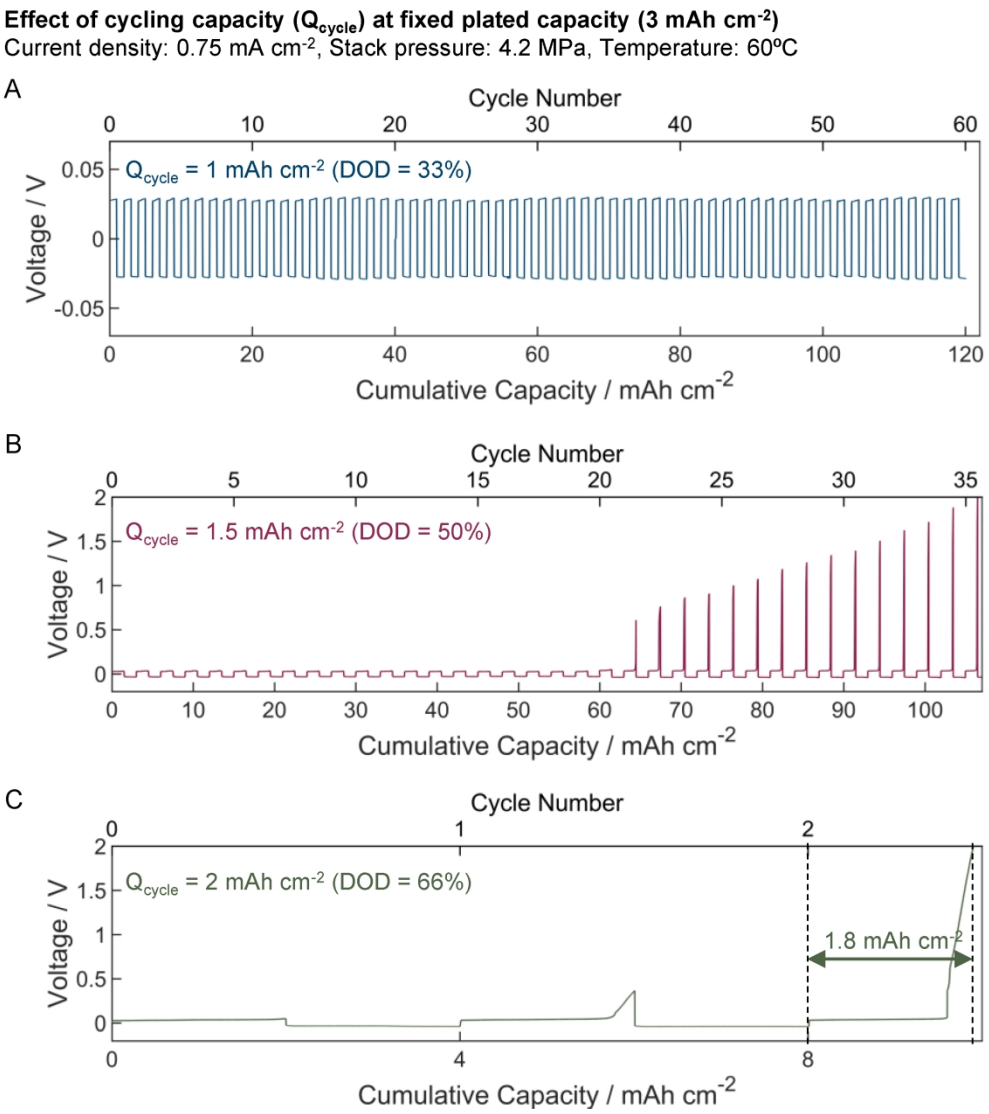

Figure 2. Effect DOD on cycling in situ Li at a fixed in situ plated capacity (3 mAh cm^{-2}). Voltage profiles when cycling (A) 1 mAh cm^{-2}, (B) 1.5 mAh cm^{-2} and (C) 2 mAh cm^{-2}; the corresponding DODs were 33%, 50% and, 66% respectively. The cell configuration is described in Figure 1 and the in situ plated Li electrodes all had an initial plated capacity of 3 mAh cm^{-2}. All the tests were conducted at 60°C and 4.2 MPa, and the current density of 0.75 mA cm^{-2} was used.

120x134mm (600 x 600 DPI)

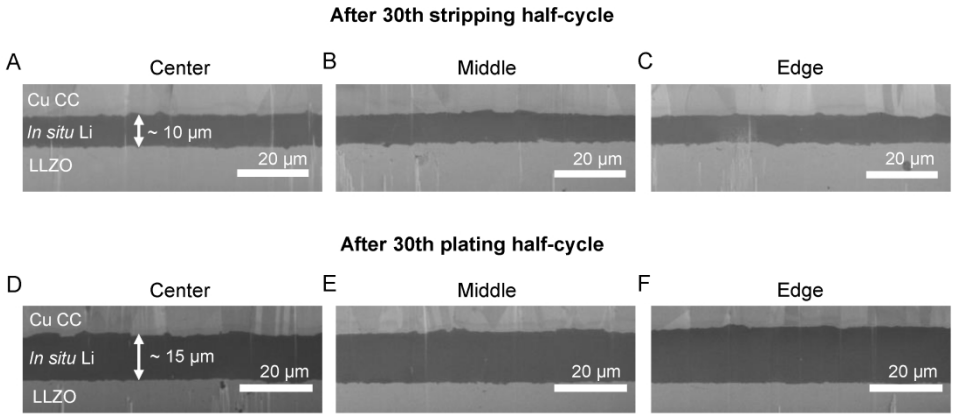

Figure 3. Li/LLZO interfaces when cycling with a DOD of 33%.(A-C) Cross-sectional SEM images of Li/LLZO interfaces after the 30th stripping half-cycle at the (A) center, (B) middle and (C) edge of the electrode. (D-E) Cross-sectional SEM images of Li/LLZO interfaces after 30th plating half-cycle at the (D) center, (E) middle and (F) edge of the electrode.

140x59mm (600 x 600 DPI)

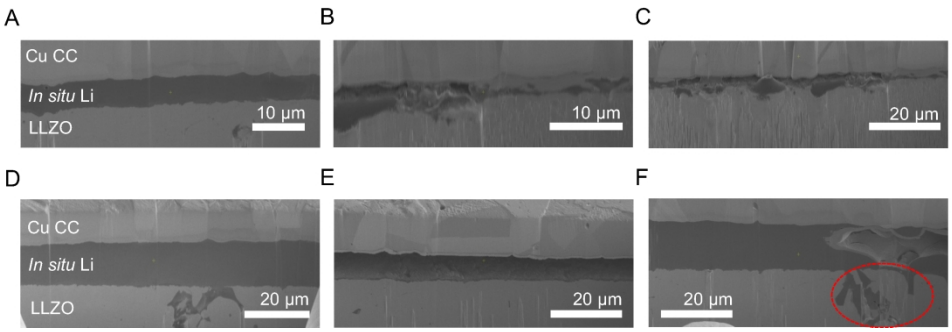

Figure 4. Li/LLZO interfaces when cycling at a DOD of 66%.(A-C) Cross-sectional SEM images of the cell after dramatic increase in voltage was observed. (D-F) Cross-sectional SEM images of the cell after plating Li on voided/de-wetted interfaces. (D) Uniform plating of Li. (E) Complete depletion of Li. (F) Large void formation and Li filament penetration to LLZO.

140x46mm (600 x 600 DPI)

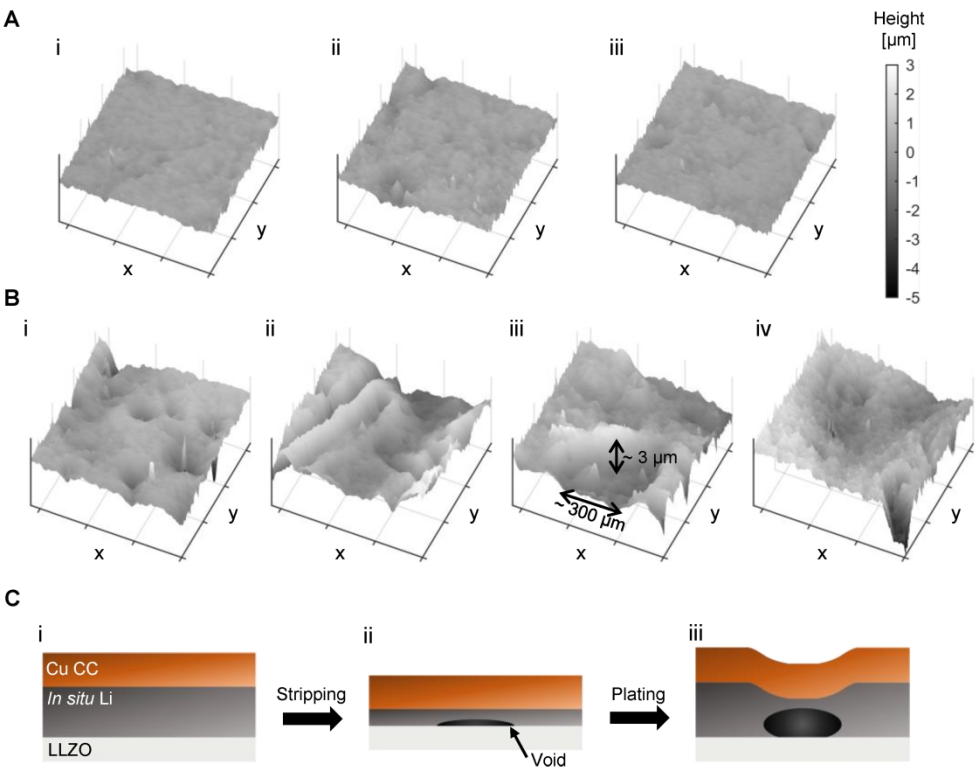

Figure 5. Surface morphologies of a Cu CC before (top row) and after (bottom row) cycling. 3D images of surface of the Cu CC (A) after *in situ* plating and (B) after cycling at a DOD of 66%. Each tick of x and y axis represents 200 µm. Each investigated area was 650 x 650 μm^2 (0.42 mm^2). (C) Schematic illustration of the formation of inhomogeneous Li during cycling.

140x109mm (600 x 600 DPI)

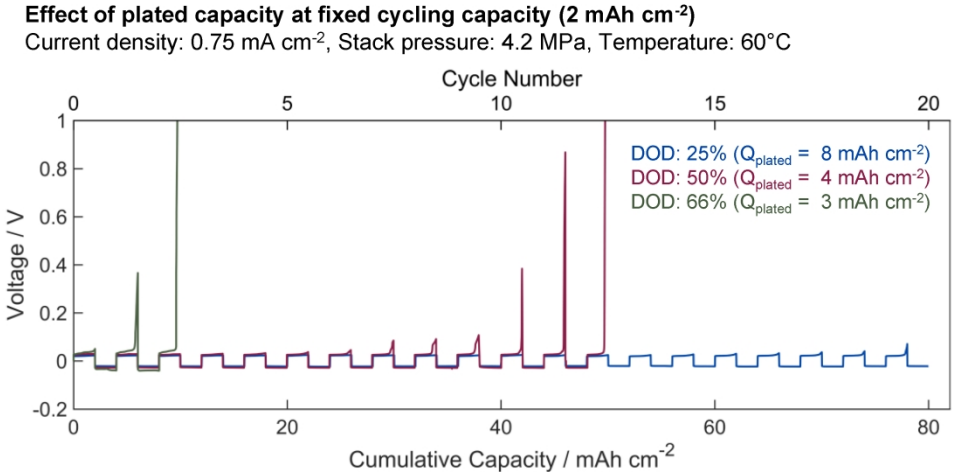

Figure 6. Effect of DOD on cycling in situ Li anodes with a fixed cycling capacity.
Voltage responses of cycling in situ Li anodes of 2 mAh cm^{-2} at different DOD by varying the amount of initially in situ plated Li (3 mAh cm^{-2} in orange, 4 mAh cm^{-2} in red and 8 mAh cm^{-2} in blue).

140x67mm (600 x 600 DPI)

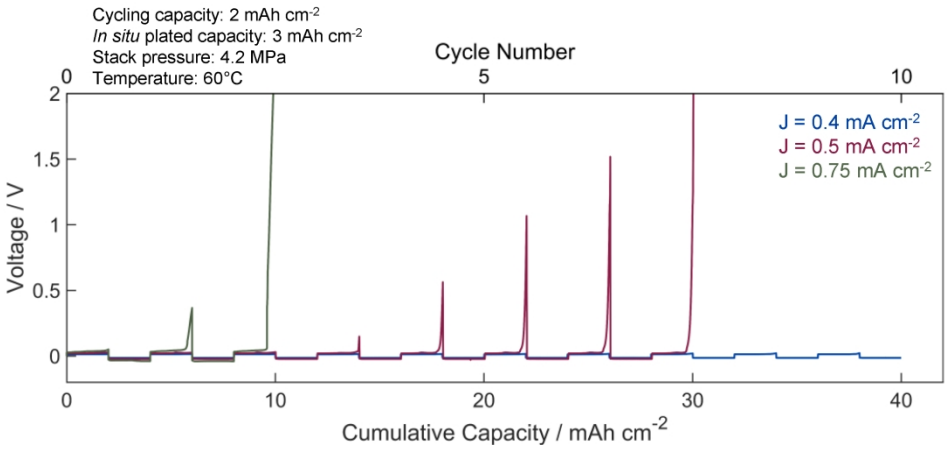

Figure 7. Effect of current density in cycling in situ Li.
Voltage profiles when 2 mAh cm^{-2} was cycled after in situ plating of 3 mAh cm^{-2} at the current density of 0.4 (blue), 0.5 (red) and 0.75 mA cm-2 (orange).

140x62mm (600 x 600 DPI)